Journal of Medicinal Chemistry

ARTICLE

pubs.acs.org/jmc

Design, Synthesis, and X-ray Crystallographic Studies of α-Aryl Substituted Fosmidomycin Analogues as Inhibitors of *Mycobacterium tuberculosis* 1-Deoxy-D-xylulose 5-Phosphate Reductoisomerase†

Mounir Andaloussi,[‡,#] Lena M. Henriksson,[§,#] Anna Więckowska,[‡] Martin Lindh,[‡] Christofer Björkelid,[§] Anna M. Larsson,[§] Surisetti Suresh,[‡] Harini Iyer,[⊥] Bachally R. Srinivasa,[⊥] Terese Bergfors,[§] Torsten Unge,[§] Sherry L. Mowbray,[∥,§] Mats Larhed,[‡] T. Alwyn Jones,[§] and Anders Karlén*[,‡]

[‡]Organic Pharmaceutical Chemistry, Department of Medicinal Chemistry, Uppsala University, Biomedical Center, Box 574, SE-751 23 Uppsala, Sweden

[§]Department of Cell and Molecular Biology, Uppsala University, Biomedical Center, Box 596, SE-751 24 Uppsala, Sweden

[∥]Department of Molecular Biology, Swedish University of Agricultural Sciences, Biomedical Center, Box 590, SE-751 24 Uppsala, Sweden

[⊥]AstraZeneca India Private Limited, Bellary Road, Hebbal, Bangalore 560024, India

Supporting Information

ABSTRACT: The natural antibiotic fosmidomycin acts via inhibition of 1-deoxy-D-xylulose 5-phosphate reductoisomerase (DXR), an essential enzyme in the non-mevalonate pathway of isoprenoid biosynthesis. Fosmidomycin is active on *Mycobacterium tuberculosis* DXR (*Mt*DXR), but it lacks antibacterial activity probably because of poor uptake. α-Aryl substituted fosmidomycin analogues have more favorable physicochemical properties and are also more active in inhibiting malaria parasite growth. We have solved crystal structures of *Mt*DXR in complex with 3,4-dichlorophenyl substituted fosmidomycin analogues; these show important differences compared to our previously described forsmidomycin−DXR complex. Our best inhibitor has an IC_{50} = 0.15 μM on *Mt*DXR but still lacked activity in a mycobacterial growth assay (MIC > 32 μg/mL). The combined results, however, provide insights into how DXR accommodates the new inhibitors and serve as an excellent starting point for the design of other novel and more potent inhibitors, particularly against pathogens where uptake is less of a problem, such as the malaria parasite.

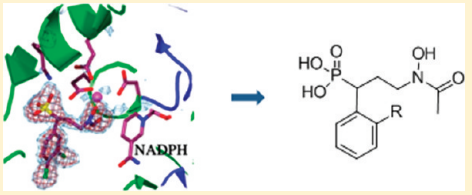

INTRODUCTION

Tuberculosis, one of the oldest diseases known, is caused by an infection with the bacterium *Mycobacterium tuberculosis*. The seriousness of tuberculosis is underlined by the fact that the World Health Organization (WHO, http://www.who.org) in 1993 took the unprecedented step of declaring the disease a global emergency. The WHO estimates that *M. tuberculosis* currently infects one-third of the world's population and caused 1.7 million deaths in 2009. The search for new drugs and the identification of suitable new drug targets have become even more urgent because of the emergence of drug-resistant and multidrug-resistant strains.

Isopentenyl diphosphate (IPP), the precursor of the highly diversified group of essential isoprenoids,[1] is synthesized through the non-mevalonate pathway in plants, protozoa, green algae, and many bacteria,[2−4] starting from pyruvate and D-glyceraldehyde 3-phosphate. In other eukaryotes as well as archaea,[5] IPP is instead formed through the classical mevalonate pathway,[6] starting from acetyl-CoA. The different routes used for IPP synthesis suggest that all enzymes within the non-mevalonate pathway are potentially interesting targets for new drugs against many pathogens, including *M. tuberculosis*. Indeed, studies have shown that all the enzymes within this pathway are essential in *Bacillus subtilis*.[7] In the second step, 1-deoxy-D-xylulose 5-phosphate reductoisomerase (DXR, also referred to as IspC; EC 1.1.1.267) catalyzes the NADPH-dependent rearrangement and reduction of 1-deoxy-D-xylulose 5-phosphate (DXP) to form 2-*C*-methyl-D-erythritol 4-phosphate (MEP), a reaction that also requires the presence of a divalent cation such as Mg^{2+}, Co^{2+}, or Mn^{2+}.[8] Knockouts of the *dxr* gene in *Escherichia coli* are lethal,[9] and the essentiality of the *M. tuberculosis dxr* gene for growth in vitro has also been demonstrated.[10]

The natural antibiotic fosmidomycin (Figure 1) is a known inhibitor of the non-mevalonate pathway in plants and bacteria.[12,13] The compound has been shown to efficiently inhibit DXRs from *E. coli*[14] (*Ec*DXR) and the malaria parasite *Plasmodium falciparum*[11] (*Pf*DXR), and the activities of various fosmidomycin analogues on these two enzymes seem to be well correlated.[15] Furthermore, fosmidomycin has antibacterial activity on *E. coli*[10,14] and can inhibit the growth of *P. falciparum* in cell culture.[11,16] The acetyl derivative of fosmidomycin, 3-(*N*-hydroxyacetamido)-1-propylphosphonic acid **2** (FR900098, Figure 1), has also been evaluated in many studies and shown to be twice as

Received: January 4, 2011
Published: June 16, 2011

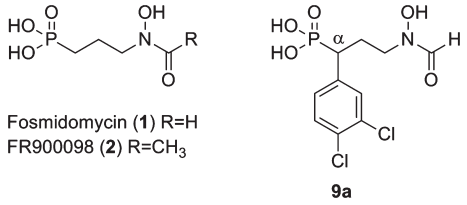

Figure 1. Structures of fosmidomycin, FR900098,[11] and the 3,4-dichlorophenyl-substituted fosmidomycin analogue.

active as fosmidomycin against *P. falciparum* in vitro and in the *P. vinckei* mouse model.[11] A number of clinical studies have demonstrated that fosmidomycin in combination with clindamycin has efficacy and good tolerability in the treatment of *P. falciparum* malaria.[17−19]

In 2005, Dhiman et al.[20] showed that fosmidomycin inhibits *M. tuberculosis* DXR (*Mt*DXR) with an IC_{50} of 0.31 μM but has no effect on *M. tuberculosis* cell growth. The antibacterial activity of fosmidomycin on *E. coli* has been shown to rely on a cAMP-dependent glycerol 3-phosphate transporter that allows uptake in that organism[21] but that seems to be lacking in *M. tuberculosis*. The absence of activity on *M. tuberculosis* is not due to the presence of exporters or to modification of fosmidomycin inside the cell.[10] Since the lack of uptake of this compound into the mycobacterial cell most likely results from its polar character, it would be of interest to explore analogues of fosmidomycin with modified hydrophobic/hydrophilic properties as potential antimycobacterial drugs, similar to the approach followed in the pursuit of more bioavailable antimalarial agents. These include modifications of the phosphonate group that yield phosphonate prodrugs expected to enhance oral availability.[22,23] Different acyl group substituents have also been prepared, as well as modifications of the hydroxamate group and of the three-carbon spacer (see, for example, refs 24−26 and other work cited therein). Although such analogues have not been evaluated on *Mt*DXR activity or in *M. tuberculosis* whole cell growth assays, the SAR obtained from the published studies can be used as a starting point for the development of *Mt*DXR inhibitors. The conserved nature of the DXR active site suggests that newly synthesized inhibitors may show broad-spectrum activity against a range of pathogens.

No analogues have yet been synthesized that have been shown to be significantly more potent than fosmidomycin or **2** on either *Ec*DXR or *Pf*DXR. Therefore, it was interesting when Haemers et al.[27] showed that several α-aryl-substituted fosmidomycin analogues were more effective than fosmidomycin in inhibiting the malaria parasite's growth. The 3,4-dichlorophenyl-substituted analogue (Figure 1) was the most potent in the series. The authors speculated that the improved in vitro antimalarial activity could be due to either an improved interaction with *Pf*DXR (compared to *Ec*DXR) or the electronic and lipophilic properties of the substituent or alternatively that the aromatic ring in the Cα-position facilitated entry into the parasite cells. Recently, it was suggested[25] that the electron withdrawing properties of the 3,4 dichlorophenyl group lower the pK_a of the phosphonate group, thereby favoring the doubly ionized form that seems to be beneficial for activity.[28,29] The improved activity against the parasite prompted us to first resynthesize this compound (**9a**) and its acetyl derivative (**9c**), as well as their monoethyl and diethyl phosphonate esters, and to evaluate the activity of the various analogues on *Mt*DXR and on *M. tuberculosis* cell growth. In parallel studies, we determined crystal structures of *Mt*DXR in complex with two such analogues, which show some similarities to, but also important differences from, fosmidomycin binding. These structures provided new insights for the design and synthesis of additional novel inhibitors.

Table 1. Structures and Inhibition Data for the 3,4-Dichlorophenyl-Substituted Fosmidomycin Analogues[a]

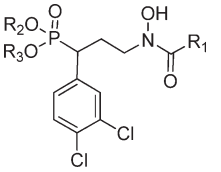

				IC_{50} (μM)	
compd	R_1	R_2	R_3	*Mt*DXR	*Ec*DXR[27]
8a	H	Et	Et	>100	Nt
8b	CH_3	Et	Et	>100	Nt
9a	H	H	H	0.15 ± 0.02	0.059 ± 0.020
9b	H	Et	H	38 ± 18	Nt
9c	CH_3	H	H	0.7 ± 0.1	0.119 ± 0.019
9d	CH_3	Et	H	22 ± 7	Nt
fosmidomycin (**1**)				0.08 ± 0.02	0.030 ± 0.008
2				0.16 ± 0.03	0.030 ± 0.008

[a] Nt = not tested.

RESULTS AND DISCUSSION

Synthesis and Biochemical Evaluation of 8a, 8b, and 9a−d. We prepared both formyl (**9a**) and acetyl derivatives (**9c**) of the Cα-substituted analogues. Furthermore we prepared the monoethyl (**9b**, **9d**) and diethyl phosphonate esters (**8a**, **8b**) of these analogues (Table 1). The compounds could be synthesized as racemic mixtures in good yield according to published procedures[30] and as described below (Scheme 1). The inhibitory capacity of the analogues was evaluated in a spectrophotometric assay, in which the *Mt*DXR-catalyzed NADPH-dependent rearrangement and reduction of DXP to form MEP are monitored at 340 nm (see Experimental Section). The compounds were also tested for activity against the growth of *M. tuberculosis* strain H37Rv in a microplate Alamar blue assay.

Fosmidomycin and **2** were included as reference compounds in this study. The IC_{50} of **2** has to our knowledge not previously been reported for *Mt*DXR; here we show it to be half as potent as fosmidomycin. The IC_{50} values for some of these inhibitors on *Ec*DXR have been published[27] and are included for comparison in Table 1. Compounds **9a** and **9c** had IC_{50} values of 0.15 and 0.7 μM, respectively, on *Mt*DXR. These can be compared with IC_{50} values of 0.06 and 0.12 μM on *Ec*DXR;[27] inhibition data are not available for these compounds on *Pf*DXR. The IC_{50} values of the monoethyl esters **9b** and **9d** were significantly poorer, 38 and 22 μM, respectively, while the diesters **8a** and **8b** lacked activity (IC_{50} > 100 μM). This is consistent with previous findings for *Ec*DXR; molecules with two charges on the phosphonate moiety are the most active, while activity falls when one of the charges is removed, and the uncharged molecule is inactive.[29] The reasons for the progressive decrease in activity are probably steric as well

dx.doi.org/10.1021/jm2000085 |J. Med. Chem. 2011, 54, 4964–4976

Scheme 1. Synthesis of α-Aryl Substituted Fosmidomycin Analogues 9a−j[a]

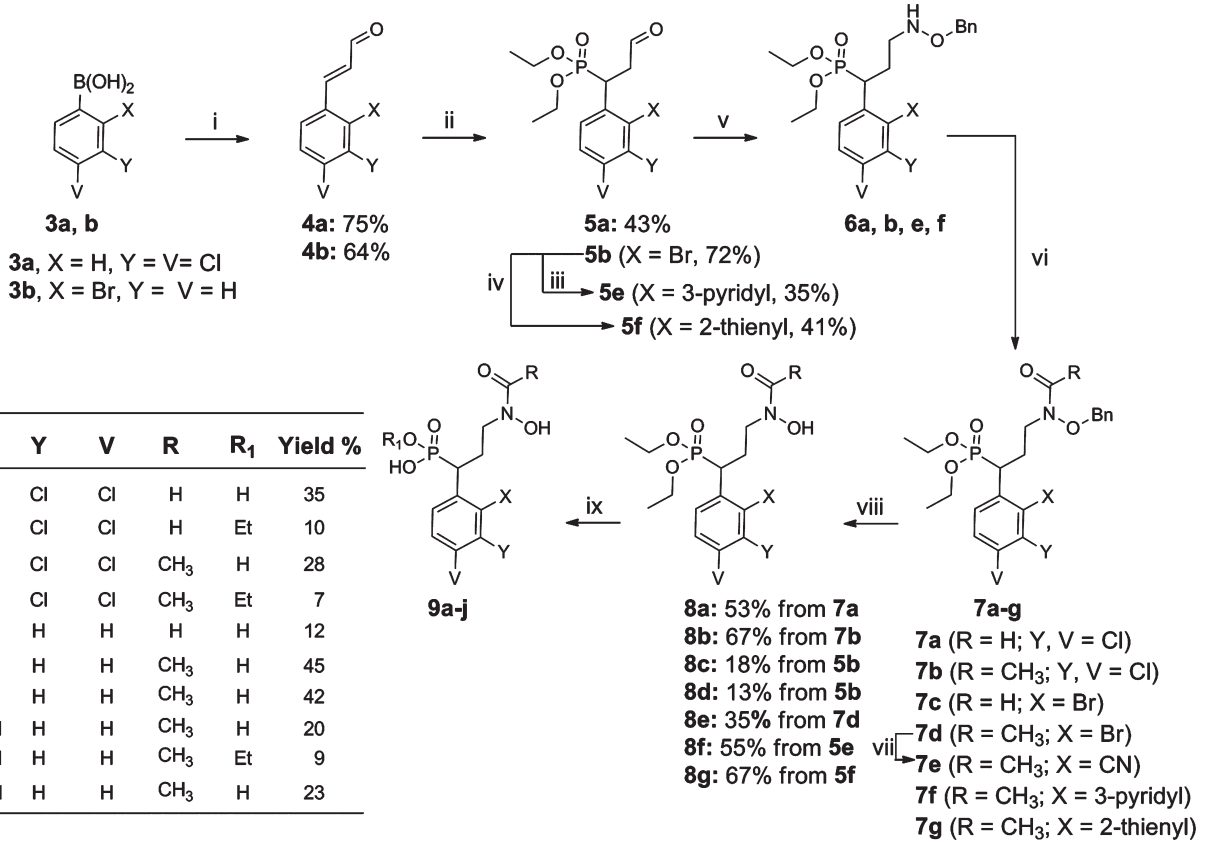

	X	Y	V	R	R_1	Yield %
9a	H	Cl	Cl	H	H	35
9b	H	Cl	Cl	H	Et	10
9c	H	Cl	Cl	CH_3	H	28
9d	H	Cl	Cl	CH_3	Et	7
9e	Br	H	H	H	H	12
9f	Br	H	H	CH_3	H	45
9g	CN	H	H	CH_3	H	42
9h	3-pyridyl	H	H	CH_3	H	20
9i	3-pyridyl	H	H	CH_3	Et	9
9j	2-thienyl	H	H	CH_3	H	23

[a] Reagents and conditions: (i) $Pd(OAc)_2$, acrolein, dmphen, *p*-benzoquinone, 100 °C, microwave; (ii) a) TEP, phenol, 100 °C; b) 2 M HCl, acetone, 100 °C; (iii) 3-pyridine boronic acid, $Pd(P\text{-}t\text{-}Bu_3)_2$, K_2CO_3, H_2O/DME, 130 °C; (iv) 2-thiophene boronic acid, $Pd(OAc)_2$, $[(t\text{-}Bu)_3PH]BF_4$, H_2O/DME 100 °C; (v) (a) *O*-benzylhydroxylamine, pyridine, EtOH, room temperature; (b) $NaCNBH_3$, MeOH, HCl, room temperature; (vi) carbonyldiimidazole, HCOOH, DCM or triethylamine, acetyl chloride, DCM, room temperature; (vii) $Zn(CN)_2$, $Pd(OAc)_2$, $[(t\text{-}Bu)_3PH]BF_4$, DMF, microwave, 140 °C; (viii) H_2, 10% Pd/C or BCl_3, DCM, −50 °C (for **8c**); (ix) TMSBr, DCM, room temperature.

as electrostatic; our earlier structural results showed that the phosphonate group interacts with a cluster of *Mt*DXR side chains and with a number of water molecules that lead out to the solvent continuum.[31] It was encouraging, however, to see that there is room for at least one ethyl group in the *Mt*DXR phosphonate binding site (**9b** and **9d**) that can be used to increase the general lipophilicity of such inhibitors. Because the predicted lipophilicity of these compounds is higher than for fosmidomycin (ClogP(fosmidomycin) = −1.8 and ClogP(**9a**) = 1.2) and since they are active on the parasite assay, it was anticipated that they could show some activity on *M. tuberculosis* cell growth. However, all six compounds had MIC > 32 μg/mL.

***Mt*DXR Crystal Structures.** Crystallographic studies were initiated in parallel to reveal the mode of binding of the fosmidomycin analogues to *Mt*DXR and so act as a framework for the design of more potent analogues with more promising biological properties. All structural investigations to date have shown that DXR exists as a homodimer. Each subunit consists of three domains, an N-terminal NADPH binding domain, a C-terminal α-helical domain, and a catalytic domain that also provides much of the dimer interface. DXRs, in general, show structural differences due to rigid-body domain motions combined with the flexibility of an active site flap. We have previously described structures of *Mt*DXR produced under two different crystallization conditions. In our first study, by use of an enzyme truncated by 20 residues at the C-terminus,[32] both magnesium sulfate and fosmidomycin were present in the crystallization, but only a sulfate ion could be located in the DXP binding site where fosmidomycin binds. After truncating the C-terminus by an additional four residues, we produced new (better and more reproducible) crystals in ammonium sulfate, which allowed us to study the binding of fosmidomycin, NADPH, and the manganese ion.[31] Since the high concentrations of sulfate might prevent weak inhibitors from binding in the active site, we here sought new crystallization conditions for the shorter construct that did not contain either sulfate or phosphate ions (see Supporting Information); this produced a third crystal form. Our second and third crystal forms both have the symmetry of space group $P2_1$ but with different unit cell parameters and are indicated in the text by $MtDXR_b$ or $MtDXR_c$. In all of our crystal forms, *Mt*DXR exists as a dimer in the crystallographic asymmetric unit, with the subunits showing some differences. In both forms b and c, we have been able to bind fosmidomycin and its analogues to the substrate-binding site of the A chain but not the B chain. Furthermore, NADPH is better defined in the cofactor binding site of the A chain, which is also more closed.[31]

We have solved the structures of the apo-enzyme in both $MtDXR_b$ and $MtDXR_c$ crystal forms. The former represents the

dx.doi.org/10.1021/jm2000085 |*J. Med. Chem.* 2011, 54, 4964–4976

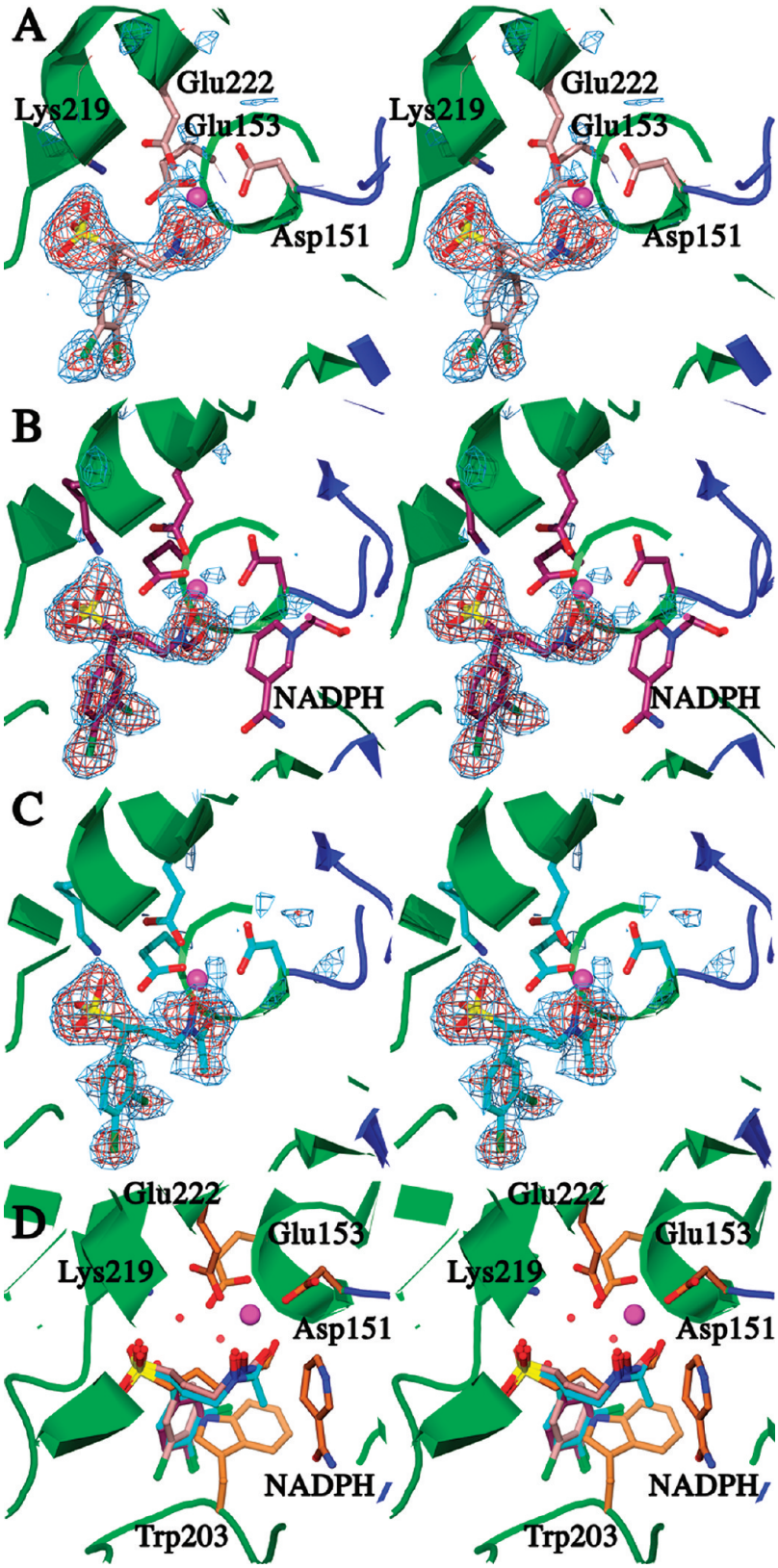

Figure 2. Stereoviews of the *Mt*DXR complexes made in the program O[34] and rendered in Molray.[35] The SIGMAA-weighted[36] $|F_o| - |F_c|$ omit maps for and around each ligand were contoured at 2.0 and 3.5 multiples of the root-mean-square (rms) value of the respective map, given in parentheses: (A) *Mt*DXRc-**9a** (rms 0.052 e/Å^3); (B) *Mt*DXRb-**9a**-NADPH (rms, 0.062 e/Å^3); (C) *Mt*DXRb-**9c** (rms 0.067 e/Å^3); (D) active site of 2JCZ (side chains and fosmidomycin in gold), with superpositioning of inhibitors from *Mt*DXRc-**9a** (pink), *Mt*DXRb-**9a**-NADPH (maroon), and *Mt*DXRb-**9c** (cyan). Water molecules lining a hydrated cavity are shown as small red spheres. In all panels, the Mn^{2+} ion is shown in magenta.

dx.doi.org/10.1021/jm2000085 |*J. Med. Chem.* 2011, 54, 4964–4976

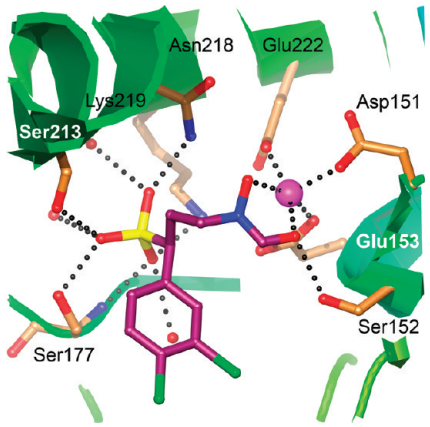

Figure 3. Interactions in the active site of *Mt*DXR$_b$-**9a**-NADPH. Protein carbon atoms are shown in gold, while those of the inhibitor **9a** are maroon. Water molecules are shown as small red spheres, and the Mn^{2+} ion is shown in magenta. Dark gray bubbles show the observed interactions.

highest resolution that we have yet achieved for this enzyme, and the latter allows us to evaluate structural changes due to the new unit cell as well as to the removal of sulfate ions from the crystallization conditions. In the apo-*Mt*DXR$_b$ A subunit, a sulfate is located in the DXP/MEP-binding site, making five interactions with protein hydrogen bond donors (Ser177 OG, Ser177 N, Ser213 OG, Asn218 ND2, Lys219 NZ) and four water molecules. In apo-*Mt*DXR$_c$, the sulfate ion is replaced by a pair of water molecules forming three hydrogen bond interactions (Asn218 ND2 for one, Ser177 N and Lys219 NZ for the other, while the Ser213 side chain rotates to form an interaction with 209 O).

Crystals of three complexes could be produced that were suitable for structural work: *Mt*DXR$_b$-**9a**-NADPH, *Mt*DXR$_c$-**9a**, and *Mt*DXR$_b$-**9c**. The A subunits of *Mt*DXR$_b$ structures can be aligned with the *Mt*DXR$_b$-fosmidomycin-NADPH structure[31] (2JCZ) with rmsd of ~0.3 Å over ~375 Cα atoms, excluding the large structural variations in the flap. The *Mt*DXR$_c$ A subunits superimpose with rmsd of 0.7 Å for 359 Cαs, while A subunits of the different crystal forms superimpose with pairwise rmsd in the range of 0.6−1.0 Å over ~360 Cα atoms. The larger deviations are the result of rigid body shifts in the C-terminal α-helical domain. Unless otherwise indicated, the electron density for the main chain of all five structures is of good quality, with the exception of the N-terminal His$_6$-tag, the first 10 residues, the active site flap of the A subunit (residues A198−A208), and residues A69−A78 in the *Mt*DXR$_c$ structures. The density for the cofactor in the *Mt*DXR$_b$-**9a**-NADPH structure is weaker than we observed in the equivalent fosmidomycin ternary complex (PDB code 2JCZ).[31] In particular, the NADPH in the B subunit is best defined for the phosphate groups and is otherwise poorly defined.

Binding of Fosmidomycin Analogues. The two fosmidomycin analogues bind in a very similar manner in the DXP/MEP site of the A chain, both in the presence and absence of NADPH (Figure 2). The detailed interactions to one of them (*Mt*DXR$_b$-**9a**-NADPH) are shown in Figure 3. As for the inhibition studies, a racemic mixture was used in the crystallographic work. Our crystallographic results indicate that **9a** and **9c** bind primarily, if not exclusively, as the *S*-enantiomers (see Supporting Information). The phosphonate group of each makes interactions with the backbone nitrogen of Ser177, as well as the side chains of Ser177, Ser213 (in one of its two possible conformations), Asn218, Lys219, and several waters. The hydroxamate group is bound in a very similar manner in each of the analogue complexes, coordinating the manganese ion and overlapping with two of the three metal-bound waters in apo-*Mt*DXR$_b$; interactions between the terminal oxygen and the side chains of Asp151 and Ser152 are also present. A sixth metal-coordinating group, the third water in apo-*Mt*DXR$_b$, is absent in the complexes because of lack of space. The dichlorophenyl ring shows some variability, including a 180° flip; electron density is weakest for the ring, which may arise from heterogeneity concerning the ring flip, from some small population of bound *R*-enantiomer, or both. Finally, the fosmidomycin propyl backbone atoms assume a very similar conformation in the three analogue structures.

Unexpectedly, the backbone conformation seen for the α-aryl fosmidomycin analogues differs from that observed for fosmidomycin itself, with two of the three torsion angles, adopting different rotamers (Figure 2D). Interestingly, our modeling of the *R*-enantiomers of **9a** and **9c** suggests that they would adopt backbone conformations more similar to fosmidomycin when binding to the active site, because of steric constraints. However, until the optically pure enantiomers of **9a** and **9c** have been prepared and evaluated, it is not possible to say if both enantiomers are active or if the binding is stereoselective. Large changes have been described previously in a particular loop near the active site of both *Mt*DXR[31] and *Ec*DXR.[33] In the present case, the most dramatic change is the fact that this flap containing Trp203 is closed (and ordered) in the fosmidomycin complex of *Mt*DXR but open in the case of the analogues described here (residues 199 to ~204 are disordered in the analogue complex structures). This difference arises because the dichlorophenyl ring of the analogues would clash with the indole ring of Trp203 if the active site flap were to adopt the closed conformation (Figure 2D). Thus, a hydrogen bond between His200 and the phosphonate group, as well as the interaction of the indole ring of Trp203 with the fosmidomycin backbone, is lost in the analogues. Further, the interaction of the hydroxamate group with the backbone nitrogen of residue 152 in fosmidomycin is lost, and only the interaction of the side chain hydroxyl group of Ser152 is maintained in the analogue complexes. This is a consequence of fosmidomycin lying ~0.5 Å deeper in the *Mt*DXR active site than the analogues. The shift also avoids clashes that would occur between the dichlorophenyl ring and Pro265. The *p*-chlorine atom and parts of the phenyl ring are partially accessible to solvent, wedged into a depression between three ordered and one disordered loop (containing residues 179, 245, 265 and 203, respectively). In the first complex structure that we solved, *Mt*DXR$_c$-**9a**, we were concerned because this edge of the dichlorophenyl ring was in contact with the active site flap from a symmetry-related copy of a B subunit (Thr202 CG2−CL atom contacts of 3.6 Å). To ensure that this had not produced a crystallographic artifact, we obtained complexes that were crystallized under other conditions, as described above. In the *Mt*DXR$_b$-**9a**-NADPH and *Mt*DXR$_b$-**9c** structures, there are no stabilizing interactions with symmetry related molecules. However, the 180° ring flip that we observe in *Mt*DXR$_c$-**9a** may indeed represent an artifact of crystal packing that allows the *m*-chlorine to pack against the symmetry molecule, instead of being buried as in the other structures (Figure 2). The extra methyl

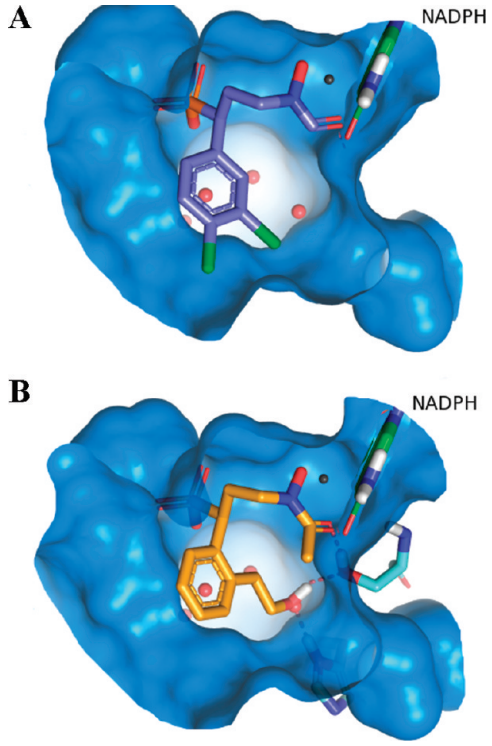

Figure 4. (A) Crystal structure of *Mt*DXR$_b$-**9a**-NADPH showing the hydrated cavity, visualized in PyMOL.[37] The protein surface is shown in blue, compound **9a** is in purple, the four waters in the hydrated cavity are in red, Mn^{2+} is in black, and the nicotinamide moiety of the NADPH cofactor is in green. (B) Compound **9n** docked in to the crystal structure of *Mt*DXR$_b$-**9a**-NADPH. The same hydrated cavity as in panel A is shown. Compound **9n** is colored yellow; coloring is otherwise as in panel A. Cavity-lining amino acid residues His248 and Ser152 are included in the panel. Possible hydrogen bonds are shown with dotted lines.

group of **9c**, compared to **9a**, is directed away from the manganese ion toward the space occupied by the indole ring of Trp203 in the closed *Mt*DXR$_b$-fosmidomycin-NADPH structure. The precise details of this potential interaction may account for the 2-fold loss in activity of **2** compared to fosmidomycin that we observe for *Mt*DXR, as opposed to *Ec*DXR, where the activities are identical.

Structure-Based Design To Investigate the Hydrated Cavity. One obvious conclusion from the structural work is that the opening of the active-site flap in the analogue-bound structures creates a large solvent-exposed region that could be explored using Cα-substitutions other than the 3,4-dichlorophenyl ring seen in our complex structures. Indeed, Haemers et al.[27] showed that analogues of **2** representing a variety of para and meta substitutions of the phenyl ring could be accommodated by *Ec*DXR with only modest differences in potency. We have previously described a hydrated cavity close to the DXP/MEP-binding site that is lined with the side chains of conserved amino acids.[31] It became apparent that this cavity could be reached from the ortho position of the 3,4-dichlorophenyl ring of **9a** (Figure 4A), which we attempted to exploit to optimize the binding of this structural class. For synthetic reasons, we prepared derivatives based on the Cα-substituted phenyl ring instead of the 3,4-dichlorophenyl moiety. Furthermore, we decided to prepare the acetyl instead of the formyl analogues, since these are generally more stable and have similar potency (e.g., comparing pairs of compounds in Table 1).

DXR is known to be a challenging protein to use in structure-based drug design, primarily because of the flexible flap and the strong substrate/inhibitor−metal interactions.[24] As a control experiment, we redocked fosmidomycin to the *Mt*DXR$_b$-fosmidomycin-NADPH structure[31] (PDB entry 2JCZ) and redocked **9a** to the *Mt*DXR$_b$-**9a**-NADPH structure, with NADPH and the manganese ion included in the complex, as described in the methods section. Each inhibitor was randomly perturbed, and after redocking, the rmsd values between the best-scored docked pose and the X-ray structure were 0.47 and 0.33 Å, respectively (heavy atoms superimposed). Encouraged by these results, we proceeded with this protocol in docking studies to evaluate an expanded set of potential inhibitors. A total of 441 synthetically feasible compounds were built based on the assumption that ortho substituents could be introduced using a Suzuki reaction starting from boronic acids and the phenyl halide. These were docked to the *Mt*DXR$_b$-**9a**-NADPH crystal structure in order to evaluate their fit to the substrate-binding pocket of the enzyme. Two compounds, one incorporating a pyridine substituent (**9h**) and one a thiophene substituent (**9j**), were chosen from these studies (see Table 2). The top-scoring docking pose of both these compounds places the ortho substituent in the hydrated cavity with the backbone adopting almost exactly the same conformations as in the *Mt*DXR$_b$-**9a**-NADPH crystal structure. However, the phenyl ring was slightly reoriented. The nitrogen in the pyridine substituent was able to hydrogen-bond to His248. The *o*-bromo substituted compound **9f**, which can be readily accessible from the common intermediate **7d**, was also evaluated.

Additionally, compounds incorporating a nitrile (**9g**), hydroxymethyl (**9k**), and hydroxyethyl group (**9n**) were suggested, with the intent of introducing a more hydrophilic group in the pocket that could displace one of the water molecules while keeping the hydrogen bonding pattern intact. Docking of these compounds into the *Mt*DXR$_b$ X-ray structure, after removal of the four water molecules, indicated that at least **9n** could participate in the water-mediated hydrogen bonding interaction with His248 (Figure 4B). The methoxymethyl **9m** and methyl **9l** compounds were intermediates in the synthetic route leading to the other compounds and were also evaluated. For comparison we also prepared the nonsubstituted Cα-phenyl analogue (**9o**). This compound was previously shown to have an IC_{50} of 0.3 μM on *Ec*DXR.[27] Finally, we prepared the cyclic phosphonate ester (**12**), a rigidified analogue that was reachable using the same synthetic route that led to **9k**.

Synthesis of Compounds 8a, 8b, 9a−o, and 12. The synthesis of the desired compounds is outlined in Schemes 1 and 2 (see also Supporting Information). The route is a modification of a previously reported method.[27] It starts with the synthesis of α,β-unsaturated aldehydes **4a** and **4b**, prepared from boronic acids **3a** and **3b** and acrolein in an oxidative Heck reaction (Scheme 1).[38] Aldehydes **4c** and **4d** were instead obtained from aryl halides and acrolein diethyl acetal using a palladium(0)-catalyzed Mizoroki−Heck reaction (Scheme 2).[39,40] 1,4-Addition of triethyl phosphite to compounds **4a**−**d** in the presence of phenol resulted in formation of the acetal intermediates, which were then hydrolyzed to aldehydes **5a**−**d**. Next compound **5b** was reacted with 3-pyridine boronic acid and 2-thiophene boronic acid in a microwave-assisted Suzuki coupling.[41] By use of the Pd(P-*t*-Bu$_3$)$_2$ catalyst in the reaction with 3-pyridine boronic acid and the Pd(OAc)$_2$/[(*t*-Bu$_3$)HP]BF$_4$ combination in

dx.doi.org/10.1021/jm2000085 |*J. Med. Chem.* 2011, 54, 4964–4976

Table 2. Inhibition of *Mt*DXR by α-Aryl-Substituted Fosmidomycin Analogues[a]

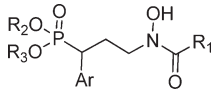

	Ar	R_1	R_2	R_3	% inhibition at 100 μM	IC_{50} (μM)
9e		H	H	H	93 ± 0.2	5.6 ± 5.9
9f		CH_3	H	H	38 ± 8	210 ± 48
9g		CH_3	H	H	30 ± 11	Nt
9h		CH_3	H	H	20 ± 10	Nt
9i		CH_3	Et	H	20 ± 5	Nt
9j		CH_3	H	H	30 ± 10	Nt
9k		CH_3	H	H	36 ± 5	465 ± 156
9l		CH_3	H	H	55 ± 6	205 ± 27
9m		CH_3	H	H	30 ± 11	Nt
9n	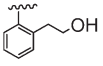	CH_3	H	H	35 ± 5	150 ± 47
9o		CH_3	H	H	92 ± 7	7.4 ± 2.6
12	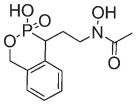				12 ± 6	Nt

[a] Nt = not tested.

the reaction with 2-thiophene boronic acid, compounds **5e** and **5f** were obtained in satisfactory yields (35% and 41%, respectively). The bromine **7d** was also used to prepare the corresponding nitrile derivative **7e** via a direct Pd-catalyzed microwave-assisted transformation using $Zn(CN)_2$.[42] In the reaction with *O*-benzylhydroxylamine and the subsequent reduction with sodium cyanoborohydride and hydrochloric acid, aldehydes **5a**−**f** were transformed into benzyloxyamines **6a**−**f**, which were then formylated (**7a**, **7c**) or acetylated (**7b**, **7d**−**i**). In order to obtain hydroxamates **8a**,**b** and **8d**−**j**, the *O*-benzyl protecting group was removed in compounds **7a**−**i** using Pd-catalyzed (10% Pd/C) hydrogenation under atmospheric hydrogen pressure. Depending on the starting material, different conditions were used for this reaction. To avoid debromination, milder conditions (ice-bath, Na_2CO_3, THF)[43] were used for compound **7d**, while compound **7g** required acidic conditions (2 M HCl, EtOH)[44] because of the thiophene substituent. When compound **7d** was subjected to Pd-catalyzed hydrogenation without any acid or base additive, both the *O*-benzyl group and aryl bromide

dx.doi.org/10.1021/jm2000085 |*J. Med. Chem.* 2011, 54, 4964–4976

Scheme 2. Synthesis of α-Aryl Substituted Fosmidomycin Analogues 9k−o and 12[a]

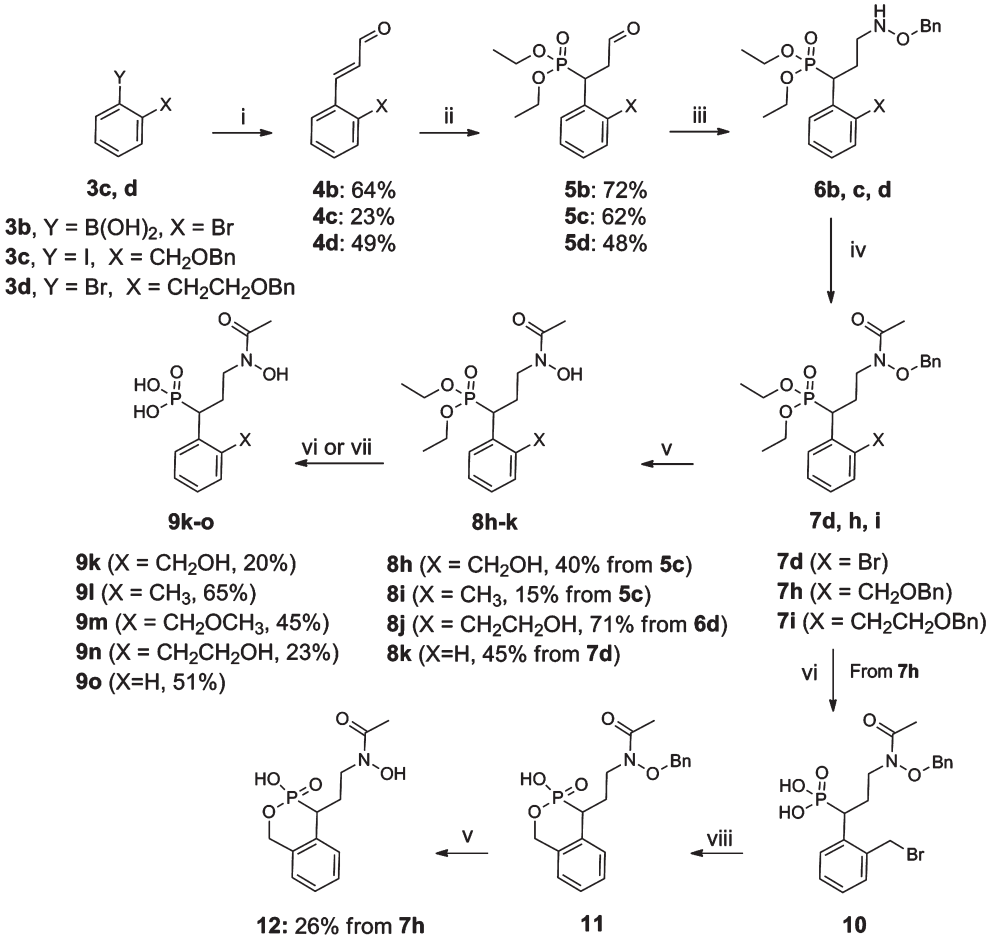

[a] Reagents and conditions: (i) $Pd(OAc)_2$, acrolein diethyl acetal, TBAA, K_2CO_3, KCl, DMF, 90 °C, microwave, 2 M HCl, reflux or $Pd(OAc)_2$, acrolein, dmphen, *p*-benzoquinone, 100 °C, microwave (for **4b**); (ii) (a) TEP, phenol, 100 °C, (b) 2 M HCl, acetone, 100 °C; (iii) (a) *O*-benzylhydroxylamine, pyridine, EtOH, room temperature; (b) $NaCNBH_3$, MeOH, HCl, room temperature; (iv) triethylamine, acetyl chloride, DCM, room temperature; (v) H_2, 10% Pd/C; (vi) TMSBr, DCM, room temperature; (vii) TMSBr, DCM, room temperature, MeOH, room temperature (from **8h** to **9m**); (viii) NaH, THF, room temperature.

underwent hydrogenolysis to obtain **8k**. The nonsymmetric dibenzyl derivative, **7h**, furnished two products in the hydrogenation reaction, that is, α-*o*-hydroxymethylphenyl and α-*o*-methylphenyl derivatives (**8h** and **8i**). In the case of **8c** the benzyl group was deprotected using 1 M BCl_3. The final step in the synthesis was hydrolysis of the phosphonate esters by bromotrimethylsilane in dichloromethane (DCM). **9e** partly undergoes deformylation under aqueous conditions. Interestingly, when compound **8h** was reacted with TMSBr, in addition to the ester hydrolysis, we also observed the formation of the *o*-bromomethyl derivative which was transformed to **9m** by reaction with MeOH.[45] We used the same approach to prepare **12**. Compound **7h** was reacted with TMSBr to give **10**, which after treatment with NaH gave the bicyclic compound **11** that after hydrogenation gave **12**. Incomplete hydrolysis of esters **8a, 8b**, and **8f**, afforded the mono ethylphosphonate esters **9b**, **9d**, and **9i** (Scheme 1). All final compounds were purified by reverse phase HPLC using gradient elution of MeOH or MeCN with 0.05% HCOOH in water.

Biochemical Evaluation of 9e−o and 12. The different analogues were evaluated for activity on *Mt*DXR (Table 2). For compounds that had more than 35% inhibition at 100 μM, we determined the IC_{50} values. First of all it is interesting to compare the IC_{50} values of **9c** and **9o**, which show that the chlorine atoms contribute some 10-fold in potency, comparable to what was found for these compounds on *Ec*DXR.[27] The bromo compound **9e** had an IC_{50} of 5.6 μM, which indicates that substitution in the ortho position is tolerated by the enzyme. However, the activity of the acetyl analogue (**9f**) dropped ~40-fold. This is a distinctly larger loss of activity than the 5-fold potency difference seen with the 3,4-dichlorophenyl substituted **9a**/**9c**, while **9d** actually has a better IC_{50} than **9b** (Table 1). A 5-fold potency difference had also been seen in the *Ec*DXR enzyme assay for the corresponding 4-MeO-phenyl substituted analogues,[27] suggesting that there may be differences in how these compounds are interacting with the enzymes. Modeling the ortho substituted bromo compound **9f** based on the structure of the **9c** complex introduces close contact clashes of the bromine atom with the OE2 atom of Glu153 or with the phosphonate group of the ligand. If the formidomycin backbone is kept fixed, these contacts can only be relieved by a dihedral rotation of the phenyl ring which eventually produces a clash between the acetyl group and the ring. No such clash would exist in the formyl

dx.doi.org/10.1021/jm2000085 |*J. Med. Chem.* 2011, 54, 4964–4976

derivative and would therefore explain the observed inhibition data. On the basis of this reasoning, substitutions at the ortho position are more likely to result in poorer inhibition for the acetyl derivative compared to the equivalent formyl compound. Indeed compounds **9g**−**j** were only weakly potent, having 20−30% inhibition at 100 μM, showing that these substituents did not improve binding. We then tried to replace one of the waters identified in the hydrated cavity of the X-ray structure with a water-mimicking group. This strategy has previously been used to increase the binding affinity of ligands, presumably because of a favorable increase in entropy associated with the release of the water molecule into the bulk solvent.[46] Docking studies, after removal of the enzyme-bound water molecules, show that the hydroxyl group of at least **9n** is able to replace one of the water molecules in the hydrated cavity (Figure 4B). However, the low activity of this compound (IC_{50} = 150 μM) indicates that it cannot effectively compete with the interactions between the water molecule and the enzyme (although **9n** is indeed more active than **9k**, which has a smaller ortho substitution). A cyclic phosphonate ester (**12**) was also prepared but lacked activity. Unfortunately, we were unable to produce crystal structures of these complexes to evaluate the accuracy of our docking and modeling experiments and to give direct experimental evidence for how the different compounds interact with *Mt*DXR. All compounds (**9e**−**o** and **12**) were evaluated for their activity against the *M. tuberculosis* strain H37Rv and shown to have MIC > 32 μg/mL.

CONCLUSIONS

Fosmidomycin should serve as an excellent starting point for the development of antitubercular drugs. Clinical trials conducted with fosmidomycin in combination with clindamycin have produced good results in the treatment of acute uncomplicated malaria, showing that *Pf*DXR is a druggable target.[47,48] Fosmidomycin is also highly active on *Mt*DXR but unfortunately lacks activity on *M. tuberculosis* whole cells, probably because of poor uptake. Therefore, one of the main challenges is to prepare modified analogues of fosmidomycin that can cross the mycobacterial cell wall. It has previously been shown that introduction of a 3,4-dichlorophenyl group in the Cα-position relative to the phosphonate group produces analogues that have a higher in vitro antimalarial activity than fosmidomycin. We resynthesized this compound and showed that it was potent on *Mt*DXR (**9a**, IC_{50} = 0.15 μM) but that it still lacked activity on *M. tuberculosis* whole cells (MIC > 32 μg/mL). Additional analogues were synthesized, which showed lower potency against the enzyme, and again, no activity was observed on mycobacterial cells. X-ray crystallographic studies were initiated in parallel, and five *Mt*DXR structures were solved, representing the apo protein as well as complexes with **9a** and **9c**, under two distinct crystallization conditions. The overall geometry of these analogues when bound to *Mt*DXR is very similar. The interactions at the phosphonate group are also very similar to those seen in the fosmidomycin−enzyme complex. However, the propyl backbone adopts a different conformation in the analogues compared to fosmidomycin. Fosmidomycin lies deeper in the active site. Although the hydroxamate groups show similar coordination to the metal ion in all cases, the analogues show a different set of hydrogen bonding interactions with protein, compared to fosmidomycin. Furthermore, the α-substituted 3,4-dichlorphenyl ring displaces the indole ring of Trp203 from the active site flap, which becomes disordered in the analogue structures. A protocol was established that could successfully redock these structures to the active site. A conserved hydrated cavity close to the binding site was explored in an effort to find compounds that would fill the cavity, perhaps displacing one of the bound water molecules. This strategy did not lead to more potent compounds, and we conclude that the structure−property relationships of fosmidomycin need to be further explored to obtain antimycobacterial activity for this structural class. However, the combined results provide key insights into how DXR responds to the binding of new inhibitors, as well as how the inhibitors themselves respond to the protein. The highly conserved DXP/MEP binding site of DXR[32] means that even if we are ultimately unsuccessful in producing compounds with antitubercular activity, we now have the basis for the design of novel, more potent inhibitors against other pathogens, such as the malaria parasite.

EXPERIMENTAL SECTION

Chemistry. The microwave reactions were performed in a Smith synthesizer producing controlled irradiation at 2450 MHz with a power of 0−300 W. The reaction temperature was determined using the built-in online IR sensor. Flash column chromatography was performed on Merck silica gel 60 (40−63 μm). Analytical thin layer chromatography was done using aluminum sheets precoated with silica gel 60 F_{254}. Analytical RPLC-MS was performed on a Gilson HPLC system with a Finnigan AQA quadrupole mass spectrometer with detection by UV (DAD) using an Onyx Monolithic C18 column (50 mm × 4.6 mm). Alternatively, a Gilson HPLC system was used with a Finnigan Thermoquest MSQ quadrupole mass spectrometer (ESI^+) and a SEDERE ELSD (Sedex 55) detector, equipped with an Onyx Monolithic C18 column (50 mm × 4.6 mm). For both systems a H_2O/CH_3CN or H_2O/CH_3OH gradient with 0.05% HCOOH was used as the mobile phase at a flow rate of 4 mL/min. Preparative RP-HPLC was performed on a system equipped with a Zorbax SB-C8 column (150 mm × 21.2 mm) using a H_2O/CH_3CN gradient with 0.1% CF_3COOH or 0.05% HCOOH as mobile phase at a flow rate of 5 mL/min. Purity of the final compounds was determined by RP-HPLC on a Dionex UltiMate 3000 binary analytical LC system using Kinetex C18 2.6 μm, 3.0 mm × 50 mm column with a H_2O/CH_3CN gradient with 0.05% HCOOH and UV detection at 214 nm. All the compounds showed purity above 95%. ^1H and ^{13}C NMR spectra were recorded on Varian Mercury Plus instruments: ^1H at 399.9 MHz and ^{13}C at 100.6 MHz or ^1H at 399.8 MHz and ^{13}C at 100.5 MHz. The chemical shifts for ^1H NMR and ^{13}C NMR are referenced to TMS via residual solvent signals (^1H, $CDCl_3$ at 7.26 ppm, CD_3OD at 3.31 ppm; ^{13}C, $CDCl_3$ at 77.16 ppm, CD_3OD at 49.00 ppm). ^{31}P spectra were recorded on a Varian Mercury 300 Plus instrument at 121.4 or 162 MHz, and the chemical shifts are referenced to 85% H_3PO_4 which was used as an external standard. Molecular masses (HR-ESI-MS) were determined on a Micromass Q-Tof2 mass spectrometer equipped with an electrospray ion source. All final products were obtained as racemic mixtures. 3-(3,4-Dichlorophenyl)acrylaldehyde (**4a**), 3-(2-bromophenyl)acrylaldehyde (**4b**), diethyl (1-(3,4-dichlorophenyl)-3-oxopropyl)phosphonate (**5a**), diethyl (1-(3,4-dichlorophenyl)-3-(*N*-hydroxyformamido)propyl)phosphonate (**8a**), diethyl (1-(3,4-dichlorophenyl)-3-(*N*-hydroxyacetamido)propyl)phosphonate (**8b**), 3-(*N*-hydroxyformamido)-1-(3,4-dichlorophenyl)propylphosphonic acid (**9a**), 3-(*N*-hydroxyacetamido)-1-(3,4-dichlorophenyl)propylphosphonic acid (**9c**), and (3-(*N*-hydroxyacetamido)-1-phenyl)propylphosphonic acid (**9o**) were previously reported.[30,49]

Materials. All reagents were purchased from commercial suppliers and used without further purification. Dichloromethane (DCM) and tetrahydrofuran (THF) were distilled under nitrogen immediately

before use. For DCM, calcium hydride was used as the drying agent. For THF, sodium/benzophenone ketyl was used as the drying agent.

(*E*)-3-(2-Bromophenyl)acrylaldehyde (4b)[49]. A test tube was charged with $Pd(OAc)_2$ (0.007 g, 0.031 mmol), 2,9-dimethyl-1,10-phenanthroline (neocuproine, dmphen) (0.006 g, 0.031 mmol) and acetonitrile (2 mL), and the mixture was stirred for 30 min at room temperature. A 2−5 mL microwave-transparent process vial was charged with acrolein (1 mL, 15.50 mmol), 2-bromophenylboronic acid (0.50 g, 3.10 mmol), *p*-benzoquinone (0.17 g, 1.55 mmol), and acetonitrile (1 mL). The content of the test tube was added to the process vial, which thereafter was capped and exposed to microwave heating for 30 min at 100 °C. After the mixture was cooled to room temperature, solvent was removed. The mixture was diluted with 0.1 M NaOH and extracted with DCM. Organic layers were then dried with anhydrous $MgSO_4$. The solvent was evaporated and the obtained crude product purified by column chromatography on silica gel (isohexane/ethyl acetate, 4/1) to yield 0.42 g (64%) of **4b**. ^{1}H NMR (400 MHz, $CDCl_3$) δ 9.69 (d, J = 7.8 Hz, 1H), 7.83 (d, J = 15.6 Hz, 1H), 7.60 (m, 1H), 7.28 (m, 2H), 7.31 (m, 1H), 6.61 (dd, J = 7.8, 15.6 Hz, 1H); ^{13}C NMR (100 MHz, $CDCl_3$) δ 193.8, 150.9, 137.8, 133.9, 132.4, 130.9, 128.3, 128.2, 126.0. MS (ESI$^+$): m/z 211 (M + H$^+$), 213 (M + 2 + H$^+$). Formula: C_9H_7BrO.

Diethyl 1-(2-Bromophenyl)-3-oxopropylphosphonate (5b). A solution of aldehyde **4b** (0.42 g, 2.00 mmol), phenol (0.49 g, 5.20 mmol), and triethyl phosphite (0.39 g, 2.40 mmol) was stirred at 100 °C for 2 h. Then the mixture was evaporated under vacuum and the obtained product was refluxed for 24 h in a mixture of acetone (17 mL), water (3 mL), and 2 M HCl (8 mL). After that time, the mixture was cooled to room temperature and extracted with diethyl ether (3 × 50 mL). The combined organic layers were dried over anhydrous $MgSO_4$, filtered, and concentrated under vacuum. The crude product was purified by silica gel column chromatography using ethyl acetate as eluent to yield 0.50 g (72%) of **5b**. ^{1}H NMR (400 MHz, $CDCl_3$) δ 9.62 (d, J = 1.6 Hz, 1H), 7.57 (d, J = 8.8 Hz, 1H), 7.59 (m, 1H), 7.28 (t, J = 7.4 Hz, 1H), 7.10 (m, 1H), 4.35 (m, 1H), 4.10 (m, 2H), 3.85 (m, 2H), 3.15 (m, 2H), 3.05 (m, 2H), 1.20 (t, J = 7.0 Hz, 6H); ^{13}C NMR (100 MHz, $CDCl_3$) δ 198.7 (d, J_{C-P} = 15.5 Hz), 135.3 (d, J_{C-P} = 5.9 Hz), 133.4, 129.9 (d, J_{C-P} = 4.4 Hz), 129.3, 128.1, 126.0 (d, J_{C-P} = 9.6 Hz), 63.3 (d, J_{C-P} = 6.6 Hz), 62.7 (d, J_{C-P} = 6.6 Hz), 44.7 (d, J_{C-P} = 2.2 Hz), 36.7 (d, J_{C-P} = 141.5 Hz), 16.6 (d, J_{C-P} = 5.9 Hz), 16.4 (d, J_{C-P} = 5.9 Hz). MS (ESI$^+$): m/z 349 (M + H$^+$), 351 (M + 2 + H$^+$). Formula: $C_{13}H_{18}BrO_4P$.

Diethyl 1-(2-Bromophenyl)-3-(*N*-hydroxyformamido)propylphosphonate (8c). A mixture of **5b** (0.47 g, 1.36 mmol) and *O*-benzylhydroxylamine hydrochloride (0.21 g, 1.36 mmol) in a solution of pyridine/ethanol, 1/1 (5.6 mL), was stirred at room temperature. After 4 h, TLC (100% ethyl acetate) indicated that the reaction was completed. The reaction mixture was evaporated and thereafter coevaporated with toluene 3 times. The obtained crude product was dissolved in methanol (20 mL) together with $NaBH_3CN$ (0.26 g, 4.10 mmol), and the solution was stirred at room temperature for 30 min. After this time the solution was cooled to 0 °C and 37% HCl (2 mL) was slowly added. The mixture was then allowed to warm to room temperature, and $NaBH_3CN$ (0.05 g, 0.90 mmol) was added; the resulting mixture was stirred for an additional 2 h. After the reaction was completed (TLC, ethyl acetate/methanol, 95/5), the mixture was basified by the addition of 10% NaOH (pH 12) and extracted with DCM. The combined organic layers were dried, filtered, and evaporated. The crude product was purified on a silica gel column (DCM/methanol 99/1) to obtain **6b** in quantitative yield. Compound **6b** (0.27 g, 0.60 mmol) dissolved in DCM (2 mL) was added to a prepared solution of formic acid (3 mL) and 1,1′-carbonyldiimidazole (0.49 g, 3.00 mmol) in DCM (5 mL). After 40 h, 60 mL of water was added, and the mixture was extracted with DCM (2 × 60 mL). The combined organic layers were dried, filtered, and concentrated. The crude product was purified by column chromatography on silica gel (EtOAc) to yield 79% of **7c**. Next a DCM solution (5 mL) of formamide **7c** (0.13 g, 0.27 mmol) was cooled to −50 °C and 1 M BCl_3 in hexane (1.1 mL, 1.10 mmol) was added dropwise under N_2 atmosphere. The contents were stirred at −50 °C for 1 h and quenched with aqueous saturated $NaHCO_3$ solution. The mixture was extracted with DCM (2 × 50 mL). The combined organic layers were dried and filtered, then concentrated. The crude product was purified using preparative RP LC−MS system with gradient elution (50−100% of acetonitrile in 0.05% aqueous formic acid) to yield 73% **8c**. ^{1}H NMR (400 MHz, $CDCl_3$) δ 8.33 and 7.64 (s, 1H), 7.52 (m, 2H), 7.32 (q, J = 7.09 Hz, 1H), 7.11 (m, 1H), 4.09 (m, 2H), 3.79 (m, 4H), 3.38 (m, 1H), 2.57 (m, 1H), 2.22 (m, 1H), 1.28 (m, 3H), 1.09 (m, 3H). MS (ESI$^+$): m/z 394 (M + H$^+$), 396 (M + 2 + H$^+$). Formula: $C_{14}H_{21}BrNO_5P$.

3-(*N*-Hydroxyformamido)-1-(2-bromophenyl)propylphosphonic Acid (9e). To a solution of phosphonate diethyl ester **8c** (75 mg, 0.19 mmol) in dry DCM (2 mL) was added TMSBr (0.1 mL, 0.76 mmol) dropwise under N_2 at 10 °C and stirred at room temperature. After 6 h the volatiles were removed under vacuum and the resulting crude product was purified using preparative RP LC−MS system with gradient elution (0−20% of acetonitrile in 0.05% aqueous formic acid). Compound **9e** was obtained in 33% yield. ^{1}H NMR (400 MHz, DMSO-d_6) δ 8.15 and 7.66 (s, 1H), 7.54 (m, 2H), 7.36 (m, 1H), 7.15 (m, 1H), 3.48 (m, 1H), 3.30 (m, 1H), 3.12 (m, 1H), 2.34 (m, 1H), 2.01 (m, 1H); ^{31}P NMR (162 MHz, DMSO-d_6) δ 23.13, 23.10 (major and minor isomer). MS (ESI$^+$): m/z 338 (M + H$^+$), 340 (M + 2 + H$^+$). Formula: $C_{10}H_{13}BrNO_5P$. HRMS: m/z found [M + H]$^+$ 337.9791, $C_{10}H_{14}BrNO_5P$ requires 337.9793.

Inhibition Assay. Inhibition of *Mt*DXR activity was measured in a spectrophotometric assay[8,31,50] by monitoring the NADPH-dependent rearrangement and reduction of DXP to form MEP, using the absorption of NADPH at 340 nm. Assay reactions had a final volume of 50 μL and contained 50 mM HEPES−NaOH, pH 7.5, 100 mM NaCl, 1.5 mM $MnCl_2$, 0.2 mM NADPH, 0.048 μM *Mt*DXR, 0.2 μM DXP, and inhibitory compound at various concentrations. For comparison, the K_m values are 7.2 μM for NADPH and 340 μM for DXP.[32] Initial screening for inhibition was performed with an inhibitor concentration of 100 μM. IC_{50} measurements were performed using six reactions with inhibitor concentrations ranging between 0.01 and 1000 μM. Reactions were initiated by adding DXP and followed simultaneously in a 96-well plate (UV-Star, Greiner) at 22 °C with a spectrophotometer (Envision 2140 multilabel reader, PerkinElmer). Absorbance at 340 nm was measured every 5 s during a 500 s period. The slope of the linear phase of each reaction was used to calculate the initial velocity. This was compared to the velocity of the uninhibited reaction and used to calculate enzyme activity. Enzyme activities were plotted against the corresponding inhibitor concentration, and data points were fitted to eq 1,

$$Y = Lo + \frac{Hi - Lo}{1 + \frac{X}{IC_{50}}} \quad (1)$$

where Hi is the estimated highest enzyme activity at zero inhibitor concentration, Lo is the estimated lowest enzyme activity at infinite inhibitor concentration, X is the concentration of inhibitor, and Y is the measured enzyme activity. IC_{50} values presented are the average of three independent experiments.

Antimycobacterial Activity. The antimycobacterial activity of the compounds was determined using a resazurin dye based assay in a 96-well V-bottomed plate format as described by Marcel et al.[51] Serially diluted compound solution was added to log phase culture of *M. tuberculosis* H37Rv (ATCC no. 27294). The growth of the bacteria was monitored over 14 days with spectrophotometric readings at 575 and 610 nm. The growth curve and MIC values were computed using XL-fit (Excel, Microsoft Corp.).

Crystallographic Work. Crystallization trials were performed at 22 °C by the hanging-drop vapor-diffusion method. Drop volumes

typically consisted of 2−4 μL of protein solution (2.8−4.4 mg/mL in the final concentration buffer,[31] 6−12 mM $MnCl_2$, 10 mM dithiothreitol) and 2−4 μL of screening solution. Drops were equilibrated against a reservoir of 1 mL of screening solution. For cocrystallization trials with either the inhibitor alone or the inhibitor and NADPH, the protein solution was mixed with at least a 10× molar excess of ligands immediately before setup. Compounds **9a** and **9c** were dissolved in 10% methanol and 100% DMSO, respectively.

Our previously reported crystals of *Mt*DXR in complex with fosmidomycin[31] (indicated by *Mt*DXR$_b$) were obtained with a screening solution consisting of 25% (w/v) PEG 3350, 0.2 M ammonium sulfate, and 0.1 M Bis-Tris, pH 5.7−5.9. Three of our new structures were grown from these same conditions. They include the apo structures of *Mt*DXR$_b$, *Mt*DXR$_b$-**9a**-NADPH, and *Mt*DXR$_b$-**9c**. Apocrystals of the protein were used to seed the cocrystallization trials. Crystals appeared within a few days and grew to average dimensions of 0.2 mm × 0.1 mm × 0.03 mm in 1−2 weeks. For data collection, the crystals were flash-cooled in liquid nitrogen after a brief soak in a cryosolution consisting of the screening solution in 25% glycerol and 75 mM NaCl. DMSO, dithiothreitol, cofactors (Mn^{2+}, NADPH), and ligands (compounds **9a**, **9c**) were also included, where appropriate, in the respective cryosolutions.

To avoid the presence of a sulfate (or phosphate) group in the DXP-binding site, a search for alternative crystallization conditions was undertaken. As above, drops were seeded 24 h after setup. Crystals of apo-*Mt*DXR appeared in 17−20% (w/v) PEG 3350, 0.2 M sodium formate, pH 7.2 (conditions indicated by *Mt*DXR$_c$). Cocrystals of *Mt*DXR$_c$-**9a** were also obtained with these new conditions. The crystals grew within 1−2 weeks to dimensions similar as those reported above. Cryosolutions were prepared in the same manner but substituting sodium formate for the ammonium sulfate. Soaking times varied from a few seconds to 12 min.

Details of the data collection and crystallographic refinement are provided in the Supporting Information. Briefly, two distinct apo structures were solved and refined at resolutions of 1.90 and 1.65 Å, with crystallographic *R*-factors of 19.8% and 18.7%, respectively. A complex of *Mt*DXR with compound **9a** alone was refined at 2.05 Å resolution (*R*-factor 21.2%), while a **9a** complex with bound NADPH was refined at 1.96 Å resolution (*R*-factor 17.4%). A complex with compound **9c** at 1.95 Å resolution (*R*-factor 18.5%) was also obtained.

Docking Study. Docking was performed using Glide[52] in XP mode with default settings. All inhibitors were docked to the A chain of *Mt*DXR$_b$-**9a**. In order to prepare the enzyme for docking, the protein preparation wizard in Maestro[53] was used with default settings. Manual corrections were made by deleting zero-order bonds to the metal, correcting the bond order of NADPH, and deleting all water molecules. Furthermore, the protonation state of His248 was adjusted so that the protonated nitrogen was oriented toward the inhibitor. The missing side chains of the active-site flap A199-A204 were added to the protein model in an open conformation. The docked compounds do not directly interact with the flexible flap, and the position of the open flap is therefore not considered to be of significance for the docking results. The docking site was defined around **9a** using the "dock ligands of similar size" setting, and three docking poses were saved for each ligand.

On the basis of the Suzuki reaction, 441 synthetically feasible compounds were created by joining compound **9a** with different boronic acids using the software Legion,[54] Tripos. Ligprep[55] was used to generate different ionization states, tautomers, and stereoisomers for each compound.

■ ASSOCIATED CONTENT

Supporting Information. Additional experimental details, spectroscopic data, cloning, protein expression and purification, and structural studies. This material is available free of charge via the Internet at http://pubs.acs.org.

Accession Codes

[†]Coordinates and structure factor data have been deposited at the Protein Data Bank with entry codes 2Y1D (*Mt*DXR$_c$-**9a**), 2Y1F (*Mt*DXR$_b$-**9a**-NADPH), 2Y1G (*Mt*DXR$_b$-**9c**), 2Y1E (*Mt*DXR$_b$), and 2Y1C (*Mt*DXR$_c$).

■ AUTHOR INFORMATION

Corresponding Author

*Phone: +46-18-4714293. Fax: +46-18-4714474. E-mail: anders.karlen@orgfarm.uu.se.

Author Contributions

[#]M. Andaloussi and L. M. Henriksson contributed equally to this work.

■ ACKNOWLEDGMENT

We thank Dr. Aleh Yahorau, Department of Pharmaceutical Biosciences, Uppsala University, Sweden, for conducting HRMS analyses. We also acknowledge the Swedish Foundation for Strategic Research (SSF), the Swedish Research Council (VR), and the EU Sixth Framework Program NM4TB CT:018 923 for financial support.

■ ABBREVIATIONS USED

DCM, dichloromethane; DMF, dimethylformamide; DME, dimethoxyethane; DXP, 1-deoxy-D-xylulose 5-phosphate; DXR, 1-deoxy-D-xylulose 5-phosphate reductoisomerase; *Ec*DXR, DXR from *Escherichia coli*; IPP, isopentenyl diphosphate; MEP, 2-C-methyl-D-erythritol 4-phosphate; *Mt*DXR, DXR from *Mycobacterium tuberculosis*; MIC, minimum inhibitory concentration; PDB, Protein Data Bank; *Pf*DXR, DXR from *Plasmodium falciparum*; rmsd, root mean square deviation; RP HPLC, reversed phase high performance liquid chromatography; SAR, structure−activity relationship; THF, tetrahydrofuran; TLC, thin layer chromatography; TMSBr, trimethylsilyl bromide; WHO, World Health Organization

■ REFERENCES

(1) Sacchettini, J. C.; Poulter, C. D. Creating isoprenoid diversity. *Science* **1997**, *277*, 1788–1789.

(2) Lichtenthaler, H. K. The 1-deoxy-D-xylulose-5-phosphate pathway of isoprenoid biosynthesis in plants. *Annu. Rev. Plant Physiol. Plant Mol. Biol.* **1999**, *50*, 47–65.

(3) Rohmer, M. The discovery of a mevalonate-independent pathway for isoprenoid biosynthesis in bacteria, algae and higher plants. *Nat. Prod. Rep.* **1999**, *16*, 565–574.

(4) Rohmer, M.; Knani, M.; Simonin, P.; Sutter, B.; Sahm, H. Isoprenoid biosynthesis in bacteria: a novel pathway for the early steps leading to isopentenyl diphosphate. *Biochem. J.* **1993**, *295*, 517–524.

(5) Boucher, Y.; Doolittle, W. F. The role of lateral gene transfer in the evolution of isoprenoid biosynthesis pathways. *Mol. Microbiol.* **2000**, *37*, 703–716.

(6) Spurgeon, S. L.; Porter, J. W. *Biosynthesis of Isoprenoid Compounds*; Wiley: New York, 1981; pp 1−46.

(7) Kobayashi, K.; Ehrlich, S. D.; Albertini, A.; Amati, G.; Andersen, K. K.; Arnaud, M.; Asai, K.; Ashikaga, S.; Aymerich, S.; Bessieres, P.; Boland, F.; Brignell, S. C.; Bron, S.; Bunai, K.; Chapuis, J.; Christiansen, L. C.; Danchin, A.; Debarbouille, M.; Dervyn, E.; Deuerling, E.; Devine, K.; Devine, S. K.; Dreesen, O.; Errington, J.; Fillinger, S.; Foster, S. J.;

Fujita, Y.; Galizzi, A.; Gardan, R.; Eschevins, C.; Fukushima, T.; Haga, K.; Harwood, C. R.; Hecker, M.; Hosoya, D.; Hullo, M. F.; Kakeshita, H.; Karamata, D.; Kasahara, Y.; Kawamura, F.; Koga, K.; Koski, P.; Kuwana, R.; Imamura, D.; Ishimaru, M.; Ishikawa, S.; Ishio, I.; Le Coq, D.; Masson, A.; Mauel, C.; Meima, R.; Mellado, R. P.; Moir, A.; Moriya, S.; Nagakawa, E.; Nanamiya, H.; Nakai, S.; Nygaard, P.; Ogura, M.; Ohanan, T.; O'Reilly, M.; O'Rourke, M.; Pragai, Z.; Pooley, H. M.; Rapoport, G.; Rawlins, J. P.; Rivas, L. A.; Rivolta, C.; Sadaie, A.; Sadaie, Y.; Sarvas, M.; Sato, T.; Saxild, H. H.; Scanlan, E.; Schumann, W.; Seegers, J.; Sekiguchi, J.; Sekowska, A.; Seror, S. J.; Simon, M.; Stragier, P.; Studer, R.; Takamatsu, H.; Tanaka, T.; Takeuchi, M.; Thomaides, H. B.; Vagner, V.; van Dijl, J. M.; Watabe, K.; Wipat, A.; Yamamoto, H.; Yamamoto, M.; Yamamoto, Y.; Yamane, K.; Yata, K.; Yoshida, K.; Yoshikawa, H.; Zuber, U.; Ogasawara, N. Essential *Bacillus subtilis* genes. *Proc. Natl. Acad. Sci. U.S.A.* **2003**, *100*, 4678–4683.

(8) Takahashi, S.; Kuzuyama, T.; Watanabe, H.; Seto, H. A 1-deoxy-D-xylulose 5-phosphate reductoisomerase catalyzing the formation of 2-C-methyl-D-erythritol 4-phosphate in an alternative nonmevalonate pathway for terpenoid biosynthesis. *Proc. Natl. Acad. Sci. U.S.A.* **1998**, *95*, 9879–9884.

(9) Rodriguez-Concepcion, M.; Campos, N.; Lois, L. M.; Maldonado, C.; Hoeffler, J. F.; Grosdemange-Billiard, C.; Rohmer, M.; Boronat, A. Genetic evidence of branching in the isoprenoid pathway for the production of isopentenyl diphosphate and dimethylallyl diphosphate in *Escherichia coli*. *FEBS Lett.* **2000**, *473*, 328–332.

(10) Brown, A. C.; Parish, T. Dxr is essential in *Mycobacterium tuberculosis* and fosmidomycin resistance is due to a lack of uptake. *BMC Microbiol.* **2008**, *8*, 78.

(11) Jomaa, H.; Wiesner, J.; Sanderbrand, S.; Altincicek, B.; Weidemeyer, C.; Hintz, M.; Turbachova, I.; Eberl, M.; Zeidler, J.; Lichtenthaler, H. K.; Soldati, D.; Beck, E. Inhibitors of the nonmevalonate pathway of isoprenoid biosynthesis as antimalarial drugs. *Science* **1999**, *285*, 1573–1576.

(12) Shigi, Y. Inhibition of bacterial isoprenoid synthesis by fosmidomycin, a phosphonic acid-containing antibiotic. *J. Antimicrob. Chemother.* **1989**, *24*, 131–145.

(13) Zeidler, J.; Schwender, J.; Mueller, C.; Wiesner, J.; Weidemeyer, C.; Beck, E.; Jomaa, H.; Lichtenthaler, H. K. Inhibition of the non-mevalonate 1-deoxy-D-xylulose-5-phosphate pathway of plant isoprenoid biosynthesis by fosmidomycin. *Z. Naturforsch., C* **1998**, *53*, 980–986.

(14) Kuzuyama, T.; Shimizu, T.; Takahashi, S.; Seto, H. Fosmidomycin, a specific inhibitor of 1-deoxy-D-xylulose 5-phosphate reductoisomerase in the nonmevalonate pathway for terpenoid biosynthesis. *Tetrahedron Lett.* **1998**, *39*, 7913–7916.

(15) Giessmann, D.; Heidler, P.; Haemers, T.; Van Calenbergh, S.; Reichenberg, A.; Jomaa, H.; Weidemeyer, C.; Sanderbrand, S.; Wiesner, J.; Link, A. Towards new antimalarial drugs: synthesis of non-hydrolyzable phosphate mimics as feed for a predictive QSAR study on 1-deoxy-D-xylulose-5-phosphate reductoisomerase inhibitors. *Chem. Biodiversity* **2008**, *5*, 643–656.

(16) Wiesner, J.; Henschker, D.; Hutchinson, D. B.; Beck, E.; Jomaa, H. In vitro and in vivo synergy of fosmidomycin, a novel antimalarial drug, with clindamycin. *Antimicrob. Agents Chemother.* **2002**, *46*, 2889–2894.

(17) Borrmann, S.; Adegnika, A. A.; Matsiegui, P. B.; Issifou, S.; Schindler, A.; Mawili-Mboumba, D. P.; Baranek, T.; Wiesner, J.; Jomaa, H.; Kremsner, P. G. Fosmidomycin−clindamycin for *Plasmodium falciparum* infections in African children. *J. Infect. Dis.* **2004**, *189*, 901–908.

(18) Borrmann, S.; Lundgren, I.; Oyakhirome, S.; Impouma, B.; Matsiegui, P.-B.; Adegnika, A. A.; Issifou, S.; Kun, J. F. J.; Hutchinson, D.; Wiesner, J.; Jomaa, H.; Kremsner, P. G. Fosmidomycin plus clindamycin for treatment of pediatric patients aged 1 to 14 years with *Plasmodium falciparum* malaria. *Antimicrob. Agents Chemother.* **2006**, *50*, 2713–2718.

(19) Oyakhirome, S.; Issifou, S.; Pongratz, P.; Barondi, F.; Ramharter, M.; Kun, J. F.; Missinou, M. A.; Lell, B.; Kremsner, P. G. Randomized controlled trial of fosmidomycin−clindamycin versus sulfadoxine−pyrimethamine in the treatment of *Plasmodium falciparum* malaria. *Antimicrob. Agents Chemother.* **2007**, *51*, 1869–1871.

(20) Dhiman, R. K.; Schaeffer, M. L.; Bailey, A. M.; Testa, C. A.; Scherman, H.; Crick, D. C. 1-Deoxy-D-xylulose 5-phosphate reductoisomerase (IspC) from *Mycobacterium tuberculosis*: towards understanding mycobacterial resistance to fosmidomycin. *J. Bacteriol.* **2005**, *187*, 8395–8402.

(21) Sakamoto, Y.; Furukawa, S.; Ogihara, H.; Yamasaki, M. Fosmidomycin resistance in adenylate cyclase deficient (cya) mutants of *Escherichia coli*. *Biosci., Biotechnol., Biochem.* **2003**, *67*, 2030–2033.

(22) Reichenberg, A.; Wiesner, J.; Weidemeyer, C.; Dreiseidler, E.; Sanderbrand, S.; Altincicek, B.; Beck, E.; Schlitzer, M.; Jomaa, H. Diaryl ester prodrugs of FR900098 with improved in vivo antimalarial activity. *Bioorg. Med. Chem. Lett.* **2001**, *11*, 833–835.

(23) Ortmann, R.; Wiesner, J.; Reichenberg, A.; Henschker, D.; Beck, E.; Jomaa, H.; Schlitzer, M. Acyloxyalkyl ester prodrugs of FR900098 with improved in vivo anti-malarial activity. *Bioorg. Med. Chem. Lett.* **2003**, *13*, 2163–2166.

(24) Silber, K.; Heidler, P.; Kurz, T.; Klebe, G. AFMoC enhances predictivity of 3D QSAR: a case study with DOXP-reductoisomerase. *J. Med. Chem.* **2005**, *48*, 3547–3563.

(25) Verbrugghen, T.; Cos, P.; Maes, L.; Van Calenbergh, S. Synthesis and evaluation of α-halogenated analogues of 3-(acetylhydroxyamino)-propylphosphonic acid (FR900098) as antimalarials. *J. Med. Chem.* **2010**, *53*, 5342–5346.

(26) Zinglé, C.; Kuntz, L.; Tritsch, D.; Grosdemange-Billiard, C.; Rohmer, M. Isoprenoid biosynthesis via the methylerythritol phosphate pathway: structural variations around phosphonate anchor and spacer of fosmidomycin, a potent inhibitor of deoxyxylulose phosphate reductoisomerase. *J. Org. Chem.* **2010**, *75*, 3203–3207.

(27) Haemers, T.; Wiesner, J.; Van Poecke, S.; Goeman, J.; Henschker, D.; Beck, E.; Jomaa, H.; Van Calenbergh, S. Synthesis of α-substituted fosmidomycin analogues as highly potent *Plasmodium falciparum* growth inhibitors. *Bioorg. Med. Chem. Lett.* **2006**, *16*, 1888–1891.

(28) Woo, Y. H.; Fernandes, R. P. M.; Proteau, P. J. Evaluation of fosmidomycin analogs as inhibitors of the *Synechocystis* sp. PCC6803 1-deoxy-D-xylulose 5-phosphate reductoisomerase. *Bioorg. Med. Chem.* **2006**, *14*, 2375–2385.

(29) Perruchon, J.; Ortmann, R.; Altenkamper, M.; Silber, K.; Wiesner, J.; Jomaa, H.; Klebe, G.; Schlitzer, M. Studies addressing the importance of charge in the binding of fosmidomycin-like molecules to deoxyxylulosephosphate reductoisomerase. *ChemMedChem* **2008**, *3*, 1232–1241.

(30) Haemers, T.; Wiesner, J.; Busson, R.; Jomaa, H.; Van Calenbergh, S. Synthesis of α-aryl-substituted and conformationally restricted fosmidomycin analogues as promising antimalarials. *Eur. J. Org. Chem.* **2006**, 3856–3863.

(31) Henriksson, L. M.; Unge, T.; Carlsson, J.; Åqvist, J.; Mowbray, S. L.; Jones, T. A. Structures of *Mycobacterium tuberculosis* 1-deoxy-D-xylulose-5-phosphate reductoisomerase provide new insights into catalysis. *J. Biol. Chem.* **2007**, *282*, 19905–19916.

(32) Henriksson, L. M.; Björkelid, C.; Mowbray, S. L.; Unge, T. The 1.9 Å resolution structure of *Mycobacterium tuberculosis* 1-deoxy-D-xylulose 5-phosphate reductoisomerase, a potential drug target. *Acta Crystallogr., Sect. D: Biol. Crystallogr.* **2006**, *62*, 807–813.

(33) Reuter, K.; Sanderbrand, S.; Jomaa, H.; Wiesner, J.; Steinbrecher, I.; Beck, E.; Hintz, M.; Klebe, G.; Stubbs, M. T. Crystal structure of 1-deoxy-D-xylulose-5-phosphate reductoisomerase, a crucial enzyme in the non-mevalonate pathway of isoprenoid biosynthesis. *J. Biol. Chem.* **2002**, *277*, 5378–5384.

(34) Jones, T. A.; Zou, J. Y.; Cowan, S. W.; Kjeldgaard, M. Improved methods for building protein models in electron density maps and the location of errors in these models. *Acta Crystallogr., Sect. A* **1991**, *47*, 110–119.

(35) Harris, M.; Jones, T. A. Molray—A Web interface between O and the POV-Ray ray tracer. *Acta Crystallogr., Sect. D: Biol. Crystallogr.* **2001**, *57*, 1201–1203.

(36) Read, R. J. Improved fourier coefficients for maps using phases from partial structures with errors. *Acta Crystallogr., Sect. A* **1986**, *42*, 140–149.

(37) DeLano, W. L. *The PyMOL Molecular Graphics System*; DeLano Scientific: Palo Alto, CA, U.S., 2002.
(38) Lindh, J.; Enquist, P. A.; Pilotti, Å.; Nilsson, P.; Larhed, M. Efficient palladium(II) catalysis under air. Base-free oxidative Heck reactions at room temperature or with microwave heating. *J. Org. Chem.* **2007**, *72*, 7957–7962.
(39) Battistuzzi, G.; Cacchi, S.; Fabrizi, G. An efficient palladium-catalyzed synthesis of cinnamaldehydes from acrolein diethyl acetal and aryl iodides and bromides. *Org. Lett.* **2003**, *5*, 777–780.
(40) Larhed, M.; Hallberg, A. Microwave-promoted palladium-catalyzed coupling reactions. *J. Org. Chem.* **1996**, *61*, 9582–9584.
(41) Wu, X. Y.; Öhrngren, P.; Ekegren, J. K.; Unge, J.; Unge, T.; Wallberg, H.; Samuelsson, B.; Hallberg, A.; Larhed, M. Two-carbon-elongated HIV-1 protease inhibitors with a tertiary-alcohol-containing transition-state mimic. *J. Med. Chem.* **2008**, *51*, 1053–1057.
(42) Alterman, M.; Hallberg, A. Fast microwave-assisted preparation of aryl and vinyl nitriles and the corresponding tetrazoles from organohalides. *J. Org. Chem.* **2000**, *65*, 7984–7989.
(43) Devreux, V.; Wiesner, J.; Jomaa, H.; Rozenski, J.; Van der Eycken, J.; Van Calenbergh, S. Divergent strategy for the synthesis of α-aryl-substituted fosmidomycin analogues. *J. Org. Chem.* **2007**, *72*, 3783–3789.
(44) Simpson, T. R.; Balestra, M.; Brown, D. G.; Dantzman, C. L.; Ernst, G. E.; Frietze, W.; Holmquist, C. R.; Kang, J.; McLaren, F. M.; Smith, R. W., Jr.; Woods, J. M. Preparation of *N*-Propynylthiophene-2-carboxamides as Alpha 7 Nicotinic Acetylcholine Receptor Modulators for the Treatment of Mental Disorders and Related Diseases. WO2007001225 (A1) 20060626, 2007.
(45) Whalley, J. L.; Oldfield, M. F.; Botting, N. P. Synthesis of [4-^{13}C]-isoflavonoid phytoestrogens. *Tetrahedron* **2000**, *56*, 455–460.
(46) Garcia-Sosa, A. T.; Firth-Clark, S.; Mancera, R. L. Including tightly-bound water molecules in de novo drug design. Exemplification through the in silico generation of poly (ADP-ribose)polymerase ligands. *J. Chem. Inf. Model.* **2005**, *45*, 624–633.
(47) Lell, B.; Ruangweerayut, R.; Wiesner, J.; Missinou, M. A.; Schindler, A.; Baranek, T.; Hintz, M.; Hutchinson, D.; Jomaa, H.; Kremsner, P. G. Fosmidomycin, a novel chemotherapeutic agent for malaria. *Antimicrob. Agents Chemother.* **2003**, *47*, 735–738.
(48) Missinou, M. A.; Borrmann, S.; Schindler, A.; Issifou, S.; Adegnika, A. A.; Matsiegui, P. B.; Binder, R.; Lell, B.; Wiesner, J.; Baranek, T.; Jomaa, H.; Kremsner, P. G. Fosmidomycin for malaria. *Lancet* **2002**, *360*, 1941–1942.
(49) Zhang, S. Y.; Tu, Y. Q.; Fan, C. A.; Yang, M.; Zhang, F. M. A $RhCl(PPh_3)_3/BF_3 \cdot OEt_2$ co-promoted direct C−C cross-coupling of alcohols at β-position with aldehydes. *Tetrahedron Lett.* **2009**, *50*, 4178–4181.
(50) Kuzuyama, T.; Takahashi, S.; Watanabe, H.; Seto, H. Direct formation of 2-C-methyl-D-erythritol 4-phosphate from 1-deoxy-D-xylulose 5-phosphate by 1-deoxy-D-xylulose 5-phosphate reductoisomerase, a new enzyme in the non-mevalonate pathway to isopentenyl diphosphate. *Tetrahedron Lett.* **1998**, *39*, 4509–4512.
(51) Marcel, N.; Nahta, A.; Balganesh, M. Evaluation of killing kinetics of anti-tuberculosis drugs on *Mycobacterium tuberculosis* using a bacteriophage-based assay. *Chemotherapy* **2008**, *54*, 404–411.
(52) *Glide*, version 55211; Schrödinger, LLC: New York, NY, 2009.
(53) *Maestro*, version 9.0; Schrödinger, LLC: New York, NY, 2009.
(54) *Legion*; Tripos: St. Louis, MO, 1998.
(55) *LigPrep*, version 2.3; Schrödinger, LLC: New York, NY, 2009.